Analysis of the Hydrogeological Conditions Affecting Fault Response to Nearby Hydraulic Fracturing

A. Yehya[1,2,*], D. Yassine[3], and E. Maalouf[4,*]

[1] Department of Civil and Environmental Engineering, Maroun Semaan Faculty of Engineering and Architecture, American University of Beirut, Lebanon

[2] Harvard John A. Paulson School of Engineering and Applied Sciences, Harvard University, Cambridge, USA

[3] Department of Mechanical Engineering, Maroun Semaan Faculty of Engineering and Architecture, American University of Beirut, Lebanon

[4] Baha and Walid Bassatne Department of Chemical Engineering and Advanced Energy, Maroun Semaan Faculty of Engineering and Architecture, American University of Beirut, Lebanon

*Corresponding author: Elsa Maalouf (em40@aub.edu.lb) and Alissar Yehya (ay36@aub.edu.lb)

Key Points:

- Fault response is not affected by the extent of the hydraulically fractured zone unless it is hydraulically connected to it.
- In distant faults, damage zones diffuse laterally indirect pore pressure perturbation and prevent pressure buildup.
- In near faults, damage zones act as conduits to diffuse direct pore pressure perturbation into the fault.

Abstract

The response of critically stressed dormant faults to fluid perturbation, by oil and gas production, has been a major public concern because of its link to induced seismicity. In this paper, we study the hydrogeological factors that affect a nearby fault response, during and after hydraulic fracturing (HF) operations, evaluated by the change in Coulomb Failure Stress (CFS) through coupling solid deformation and fluid flow. We take the Duvernay formation in Alberta, Canada as a base study case for our analysis. Our results show that the injection rate and the fault's distance to HF operations play an important role in increasing the CFS and hence the probability of fault reactivation. When the fault is far from the operations, its damage zones allow lateral diffusion and prevent pore pressure build up in its upper part, which stabilizes it. The lower part, however, will be under a lower normal stress and its failure may be triggered by an increase in shear stress. This is not the case for close faults where the damage zones act as conduits for pressure diffusion and the possible triggering failure mechanism will be the increase in pore pressure. Moreover, we show that the width of the HF zone does not affect the activation mechanisms or the stability of the fault unless it is hydraulically connected to its damage zone. Therefore, serious attention should be given to the fault position, its architecture, and the volume of fluid injected to help reduce the potential for induced seismicity from HF.

Plain Language Summary

The main cause for the induced seismic events occurring during or after hydraulic fracturing operations can be attributed to fluid diffusion and/or stress changes along the critically stressed dormant faults. This occurs when the high-pressure fluid diffuses into the pre-existing faults, leads to pressure build up or alters the overall stresses and, therefore, induces earthquakes. Different hydrogeological factors can affect the response of the pre-existing faults to hydraulic fracturing

operations. Based on our simulations of the Duvernay formation in Alberta, Western Canada, we conclude that the fault, which is far from the operations, is affected by the overall Coulomb stresses and, therefore, it is stabilized in the upper part while it is destabilized in its lower part. However, the close fault is completely destabilized due to the presence of the bordering damage zones that permits pore pressure diffusion. Additionally, the width of the hydraulically fractured zone does not affect the response of the fault unless it is hydraulically connected to its damage zones. Hence, besides avoiding known faults, operators need to give serious attention to the location of faults relative to the operations, its architecture and injection parameters to limit induce seismic events.

Keywords: Coulomb failure stress, induced seismicity, poroelasticity, hydraulic fracturing, pressure diffusion, fault.

1 Introduction

Besides natural tectonic movements, earthquakes can occur due to different anthropogenic activities. These activities that cause perturbation to the underground system can alter the pressure and stresses in the nearby dormant faults. Various case studies have attempted to understand the connection of mining (Mendecki et al., 2020) and fluid production with induced seismicity (Davies et al., 2013; Zbinden et al., 2017; van Thienen-Visser et al., 2018; Deng et al., 2020; Benson et al., 2020). Meanwhile, researchers have agreed on the effect of waste fluid disposal (Healy et al., 1968), geothermal systems (Bommer et al., 2006), oil and gas production (Chang and Segall, 2016; Suckale, 2009; Villa and Singh, 2020), and hydraulic fracturing (Bao and Eaton, 2016; Deng et al., 2016; Brudzinski and Kozłowska, 2019) on the activation of dormant faults, especially that the time of some of these operations was linked to the seismic events occurring in the respective region. Unconventional oil and gas production, including hydraulic fracturing operations, does not

always induce seismic events; however, under specific geological factors, seismicity can occur even after the cessation of operations (Rashedi and Mahani, 2016). Key parameters, such as the mechanical properties of the fault and the reservoir and the in-situ conditions, can play a significant role in increasing the probability of earthquake occurrence (Van Eijs et al., 2006; Wu et al., 2017).

In low permeability formations, conventional extraction techniques cannot economically produce oil and gas from the reservoirs. Hydraulic fracturing (HF) aims at enhancing the permeability of reservoirs and, therefore, stimulating the flow of hydrocarbons into the well (Peduzzi and Harding, 2013). In shale formations, the process is done by drilling a horizontal well followed by pressurizing a limited section of the cased well by a mixture of fluids and proppants, called fracking fluid (Davis and Fisk, 2017). Seismicity can be induced during or after the high-pressure injection of fluids for formations with existing faults due to the influence of this process on the stress and strain along the fault system (Villa and Singh, 2020).

The observed surge in the rate of seismicity in North America has been mainly attributed to the massive saltwater injection into porous formation (Frohlich, 2012). Similarly, major earthquakes, whose magnitudes ranging between 2 and 6, in Alberta Canada have been linked to the hydraulic fracturing operations occurring in localized areas (Holland, 2013). Particularly, the seismicity in the Duvernay formation near Fox Creek, Alberta, CA started in 2014, during hydraulic fracturing operations, till 2015, after the cessation of the operations (Schultz et al., 2017). The events are spatially and temporally correlated to the operations occurring in that area (Bao and Eaton, 2016). Knowing that the Duvernay formation is a prominent Shale target in Alberta, it is vital to answer questions that justify the occurrence of the seismic events there.

There are two major physical mechanisms to trigger an earthquake during fluid injection. The first mechanism is the pore pressure diffusion along permeable fractures or along the damage

zones of existing faults. This is mostly the case for the induced seismicity in the United States that occurred due to the injection of massive saltwater volumes into porous formations; the pore fluid pressure can diffuse for long distances until it reaches a critically stressed fault (Ellsworth, 2013; Schultz et al., 2014; Galloway et al., 2018). The second mechanism is caused by the stress changes due to the solid matrix response to injection or production (Ellsworth, 2013). Generally, there are two major factors that help nucleate an earthquake (Galloway et al., 2018): the presence of a nearly critical slip-oriented fault and a mean for stress perturbation on the fault past the critical condition. The first factor must have existed for an induced seismic event to occur (McClure & Horne, 2014). The ambiguity lies in the second factor which can be triggered by different, possibly man-induced, means. The perturbation can occur either by pore pressure diffusion that is transmitted along the damage zone (Yehya et al., 2018) or poroelastically through an impermeable rock matrix (Galloway et al., 2018) reactivating the existing faults and, therefore, releasing their stored strain energy (Walsh and Zoback, 2015). During hydraulic fracturing, the change in pore pressure alone is unlikely to induce seismic events (Bao and Eaton, 2016; Deng et al., 2016) because the pore pressure would require more time to diffuse along the fault and would experience changes after hours of injection, especially if the hydraulic fractures are not directly connected to the damage zone of the fault. However, the shear and normal stresses in hydraulically fractured poroelastic medium vary instantly and significantly. Consequently, both the deformation of porous solid material and the change in pore fluid pressure (also known as poroelastic effects (Rice and Cleary, 1976)), affect the steady state of the fault (Deng et al., 2016).

The up mentioned mechanisms can trigger the earthquake at the source of the stress or pressure perturbation or deep below and away from the source. Besides, events can occur shortly after the anthropogenic activity begins or after it has been ceased. However, there exist certain

hydrogeological conditions that facilitate fault reactivation (Witherspoon & Gale, 1977); these conditions need to be studied and analyzed while taking into consideration the importance of the two-way coupling between solid deformation and fluid flow. In this work, we explore the hydrogeological factors and perturbation mechanisms affecting faults' response during and/or after hydraulic fracturing operations. We mainly focus on the location of the faults, their orientation, the presence of a hydraulic connection between the HF zone and the faults, and the width of the damage zones. To assess the fault response, we estimate the change in the Coulomb Failure Stress (CFS) along two critically stressed faults, existing near the hydraulic fracturing operations using a two-dimensional finite element poroelastic model on COMSOL Multiphysics. To relate the fault response to real seismic data, we consider the case study of the Duvernay formation in Alberta, Western Canada where seismic events were reported during and after operations. The variations of the CFS along the two faults are analyzed and compared to the seismic events obtained from the observational data from December 2014 to March 2015 (Bao and Eaton, 2016). Finally, we compare the hydrogeological factors in the Duvernay formation to that of Fayetteville formation in Arkansas, US, where hydraulic fracturing operations did not induce seismic events to further link the fault response to specific favored conditions.

The paper is divided as follows. Section 2 describes the geology of the Duvernay formation, the model construction, and the parameters used. The third section explains the linear poroelastic model and the governing equations. Section 4 shows the results for the different parameters investigated in this study and a comparison between the Duvernay formation and the Fayetteville formation. Finally, section 5 sums up and concludes on the main outcomes drawn from the work.

2 Materials and Methods

We couple fluid flow and solid deformation to account for the poroelastic behavior and estimate the change in the Coulomb Failure Stress (CFS). We use a 2D plane strain model with a geometry inspired by the Duvernay formation case in Alberta, Canada, where induced seismicity is associated with HF. The choice of a 2D model is taken after assuming that the hydraulic fracturing operations occur around a horizontal well and affect a vertical planar region of relatively small width with respect to the domain. The main fractures propagate in this plane. Several horizontal wells are used to cover the reservoir region.

2.1 The Duvernay formation

The Duvernay is an Upper Devonian mud rock containing significant quartz and carbonate which makes it an attractive Shale gas target. Lithologically, Duvernay formation is composed of laminated bituminous shale, calcareous shale, and dense argillaceous limestone. It contains 443 trillion cubic feet of Natural Gas, 11.3 billion barrels of Natural Gas Liquids and 61.7 billion barrels of oil (Preston et al., 2016).

Irregular seismicity has been observed in the Duvernay formation in Alberta, Canada since December 2013 (Bao and Eaton, 2016). These events have been spatially and temporally correlated with the hydraulic fracturing activities occurring in the Upper Devonian Duvernay formation (Schultz et al., 2015). The link between these events and fracking operations was controversial at that time, where some authors (Atkinson et al., 2016) correlated the events with the saltwater disposal in Mississippian Debolt formation; however, the amount of water injected was not enough to have induced the observed seismic events (McGarr, 2014).

Seismic events were observed at the end of 2014 and early January 2015 during hydraulic fracturing operations in the Duvernay formation. Even after the cessation of the operations, three

158 sequences were also detected: S1 (January 10 till January 31), S2 (February 1 till February 18)
159 and S3 (March 9 till March 31). The distribution of the seismic events in that cluster outlines a
160 strike-slip system of two faults near the HF operations and with similar orientation (Bao and
161 Eaton, 2016) as shown in **Fig. 1.** The faults extend from the injection zone within the Duvernay
162 formation into the crystalline basement. In the simulations, we will try to detect if a correlation
163 exists between the numerically estimated positive CFS values describing the fault response and
164 the observed seismic data.
165

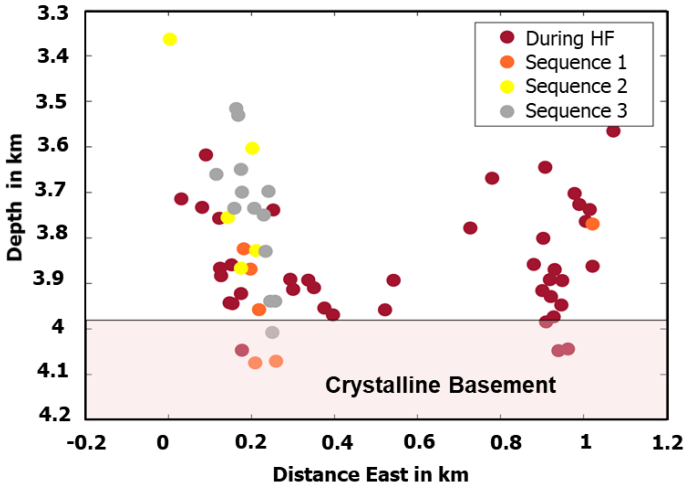

166

167 **Figure 1.** Cross section of a cluster showing the two strands of the fault system in the Duvernay
168 formation (reproduced from Bao and Eaton (2016))

169 2.2 Model construction

170 The entire domain is 10 km × 10 km divided into two layers inspired by the Alberta study case:
171 The Duvernay shale (host rock) is 4 km thick, and the crystalline basement is 6 km thick as
172 depicted in **Fig. 2**. In order to simulate the stages of the fracking operations, 15 mass sources that
173 are separated by a distance of 70 m are added at a depth of 3.4 km (Zhao, 2018) inside the

hydraulic fracturing zone (**Fig. 2a**). The hydraulic fracturing zone has a higher permeability than the host rock due to hydraulic fracturing and the permeability is considered to increase instantly during the operation. The fault system includes fault 1 (**Fig. 2b**) that is away from the hydraulic fractures, and fault 2 (**Fig. 2c**) that is directly below the hydraulic fracturing zone. Each fault has a fault core of low permeability (order of 10^{-17} m^2), and boarding damage zones of higher permeability (order of 10^{-14} m^2). The mass sources are activated one after the other by injecting 9.4 m^3/min water per mass source for 5 hours followed by 4 hours of zero-injection phase.

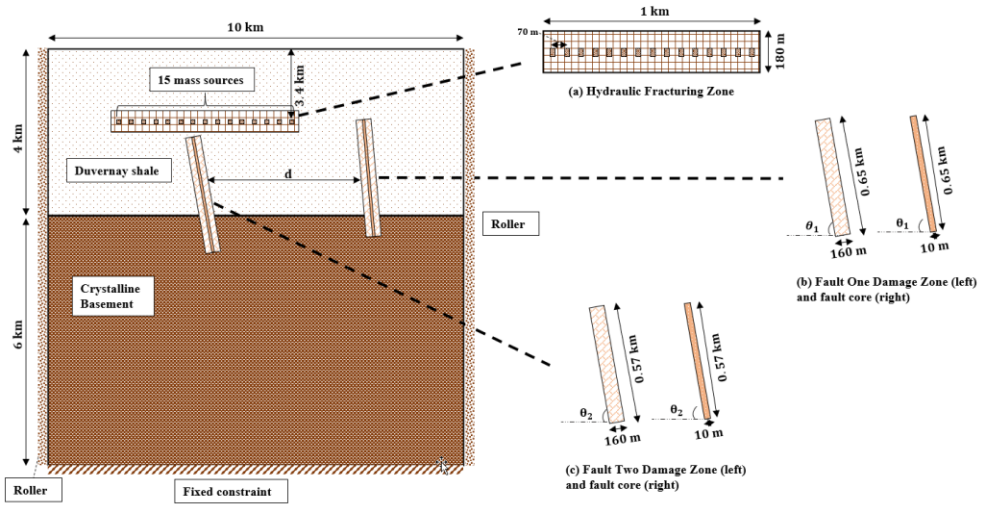

Figure 2. Model geometry with emphasis on (a) the hydraulic fracturing zone, and the geometry of (b) Fault 1 and (c) Fault 2

3 Theory and Calculations

3.1 Poroelastic model and governing equations

3.1.1 Coulomb stress changes

Generally, the change in Coulomb Failure Stress (CFS) expresses the failure criterion to initiate rupture:

$$\Delta CFS = \Delta\tau + f(\Delta\sigma_n + \Delta p) \quad \ldots(1)$$

where f is coefficient of friction, taken between 0.6 and 1, $\Delta\tau$ is the change in the shear stress, $\Delta\sigma_n$ is the change applied normal stress (positive for extension) and Δp is the change in pore pressure. Any natural or anthropogenic activity that alters the shear stress, normal stress or pore pressure can bring the fault to failure and, therefore, induce an earthquake. Hence, for a critically stressed fault, as the case of most dormant faults in the subsurface, any positive change in the CFS affect the fault response to the perturbation and could lead to fault slip.

3.1.2 Coupled poroelastic model

The coupled poroelastic model states that the change in pore pressure affects the stresses and strains (fluid-to-solid coupling) and, similarly, any change in the poroelastic stresses can lead to the variation of pore pressure (solid-to-fluid) (Biot, 1941; Rice and Cleary, 1976; Wang, 2000).

The equilibrium equation, under quasi-static condition, and no additional body forces gives:

$$\nabla . \sigma = \mathbf{0} \quad ... (2)$$

The constitutive equation of the solid matrix when pore fluid is under pressure, with the approximation of elastic isotropy, is given by:

$$G\nabla^2 \boldsymbol{r} + \frac{G}{1-2\nu} \nabla\epsilon - \alpha\nabla p = \mathbf{0} \quad ... (3)$$

where $\boldsymbol{r}$ is the displacement vector, G is the shear modulus, ν is Poisson's ratio, ϵ is the volumetric strain, α is Biot-Willis coefficient and ∇p is the applied pressure gradient.

The fluid equation, derived from the conservation of mass, requires that:

$$\frac{\partial}{\partial t}(\emptyset\rho) + \nabla . (\rho \boldsymbol{u}) = Q_m \quad ... (4)$$

where ρ is the density of the fluid, $\emptyset$ is the porosity of the medium, and Q_m is the fluid mass source.

Fluid flow in a poroelastic medium can be described by Darcy's Law where Darcy's velocity, $\boldsymbol{u}$, is expressed in terms of the permeability of the medium, κ, fluid viscosity, μ, and the difference in elevation, ∇z:

$$\boldsymbol{u} = -\frac{\kappa}{\mu}\left(\nabla p + \rho g \nabla z\right) \quad \ldots(5)$$

Furthermore, the poroelastic storage coefficient, S, is given by:

$$\frac{\partial}{\partial t}(\emptyset\rho) = \rho S \frac{\partial \rho}{\partial t} \quad \ldots(6)$$

Then, the mass conservation equation can be re-written as:

$$\rho S \frac{\partial \rho}{\partial t} + \nabla.(\rho \boldsymbol{u}) = Q_m = -\rho\alpha \frac{\partial \epsilon}{\partial t} \quad \ldots(7)$$

The negative sign in the mass source term refers to the effect of the increase of the rate of change of the volumetric strain, $\frac{\partial \epsilon}{\partial t}$. As this term increases, the fluid will sink as there is more space for the fluid to diffuse.

3.2 Initial and boundary conditions

For the initial conditions, the displacement vector is null, and the pore pressure is at hydrostatic conditions. Thus, the calculated pore pressure is the excess pressure above the hydrostatic value. As for the boundary conditions for the solid matrix, we use shear-free but impenetrable boundaries for the side and bottom boundaries described as,

$$\boldsymbol{n}\,.\,\boldsymbol{u} = 0, \qquad \boldsymbol{n} \times (\boldsymbol{\sigma}.\boldsymbol{n}) = 0 \ldots(8)$$

where $\boldsymbol{u}$ is the displacement of the solid matrix, and $\boldsymbol{\sigma}$ is the stress tensor.

The top side is free to move in any direction (traction-free) (Segall and Lu, 2015; Fan et al., 2016). For the fluid flow, we assume a zero normal component of the fluid mass flux as,

$$-\boldsymbol{n} \cdot \left(\rho \boldsymbol{v_f}\right) = 0 \ldots (9)$$

where $\boldsymbol{n}$ is the normal vector pointing outward, ρ is the fluid density, and $\boldsymbol{v_f}$ is the fluid velocity.

Table 1, **Table 2,** and **Table 3** describe the hydraulic, linear elastic and poroelastic properties of the different geological components, respectively, while **Table 4** describes the fluid properties used in the numerical models.

Table 1. Hydraulic properties of the geological components used in the numerical models

Component	**Permeability** $(\mathbf{m^2})$	**Porosity (-)**	**Reference**
Duvernay shale	$1.5\ \mathrm{E}-19$	0.65	(Kleiner and Aniekwe, 2019)
Crystalline basement	10^{-21}	0.01	(Stober and Bucher, 2014)
Hydraulic fracturing zone	10^{-16}	0.1	(Rodríguez-pradilla, 2018)
Damage zones	10^{-14}	0.1	(Yehya et al., 2018)
Fault core	10^{-17}	0.015	

Table 2. Linear elastic properties of the geological components used in the numerical models

Component	Young's Modulus (GPa)	Poisson's Ratio (-)	Density (kg/m^3)	Reference
Duvernay shale	75	0.25	2700	
Crystalline basement	60	0.2	2750	(Zhao, 2018)
Damage zones	25	0.25	2700	(Gudmundsson,
Fault core	5	0.25	2700	2004)

Table 3. Poroelastic property of the geological components used in the numerical models

Component	Biot-Willis coefficient (-)	Reference
Duvernay shale	0.79	(Fan et al., 2019)
Crystalline basement	0.44	

Table 4. Fluid properties used in the numerical models

Fluid properties	Value
Density (kg/m^3)	1000
Dynamic viscosity ($Pa.s$)	0.0004
Compressibility ($1/Pa$)	$4\ E-10$

4 Results and Discussion

In this section, we discuss the possible hydrogeological factors that affect the faults' response, which can lead to triggering the seismic events observed in the Duvernay formation.

We evaluate and analyze the effect of the several parameters on the change of Coulomb Failure Stress along the two critically stressed faults: Fault 1 and 2 and, then, correlate the change in CFS with the observed seismic events during hydraulic fracturing (HF), S1, S2 and S3. The change in CFS, pore pressure and the stresses are evaluated at the end of each sequence. The parameters that are varied are fault orientation, presence of hydraulic fracturing zone and its intersection with the damage zones, the distance to the HF operations and the width of the bordering damage zones of Fault 1.

4.1 Fault orientation

The orientations of the faults play a significant role in their stabilization state. To evaluate the effect of fault orientation on the change in CFS, Fault 1 and Fault 2 are oriented based on the observed seismic strands depicted in **Fig. 1** where $\theta_1 = 74^o$ and $\theta_2 = 84^o$ (Bao and Eaton, 2016). The model parameters shown in **Table 1**, **Table 2** and **Table 3** are adopted and the distance between the faults is 1.5 km**.** Therefore, Fault 1 is 1.01 km away from the hydraulic fracturing operations while Fault 2 is 0.425 km below the hydraulic fractures.

Fig. 3a shows the variation of the change in CFS along oriented Fault 1 during HF, S1, S2 and S3. As depicted, Fault 1 is stabilized at the shallower parts (negative CFS) and destabilized at the deeper parts (positive CFS). **Fig. 4a** shows that the shallower part of Fault 1 is subjected to a higher normal compressive stress relative to the deeper section; this leads to the destabilization of its deeper section. **Fig. 4a** shows the insignificant effect of pore pressure on the variation of CFS at the later stages of the operations along Fault 1. The distance between Fault 1 and the hydraulic fractures, which is 1.01 km, is large enough to limit a sufficient pore pressure diffusion into the fault. Therefore, the main mechanism affecting fault response, which leads to induced seismicity in the deep layers of Fault 1, is the increase in shear stress rather than pore pressure

diffusion. The observed seismic events (**Fig. 1**) occurred solely during HF at a depth of 3.6 km, which agrees with the positive CFS values in the simulation results occurring at around a depth of 3.7 km. On the other hand, **Fig. 3b** confirms that Fault 2 shows a completely destabilizing behavior in all 4 stages. During HF, pore pressure directly diffuses along Fault 2 due to its proximity to the hydraulic fracturing operations. However, the overall coulomb stresses play a significant role in destabilizing Fault 2 during the time of S1, S2 and S3 (**Fig. 4b**) where the effect of the shear and normal stresses dominated that of the pore pressure. By the time the hydraulic fracturing operations are ceased, pore pressure has already diffused along Fault 2 and, therefore, the overall stresses are the reason behind the destabilization of the fault.

In case the faults were vertical, the shear stress along both faults decreases and, therefore, the faults are more stabilized in comparison to when they are oriented (**Fig. 5**). In such case, Fault 1 becomes destabilized at a depth higher than 3.7 km. Similarly, Fault 2 is still completely destabilized; however, it exhibits higher values of CFS. Hence, the orientation of the faults did not affect the mechanisms of faults response but the location of the expected instability.

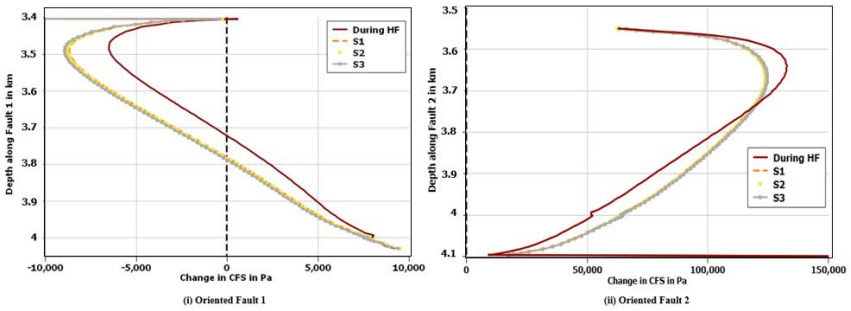

Figure 3. The variation of the CFS during the 4 stages (HF, S1, S2, S3) along the oriented faults: (a) Fault 1 and (b) Fault 2

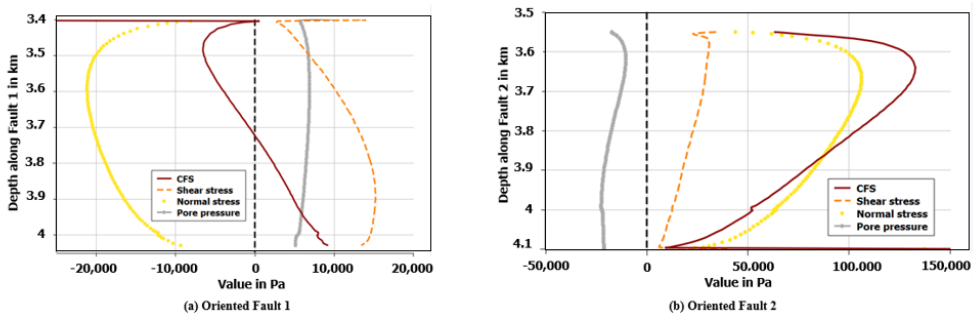

296

297 **Figure 4.** The variation of CFS, shear stress, normal stress, and pore pressure along (a) oriented

298 Fault 1 during HF and (b) oriented Fault 2 during S1

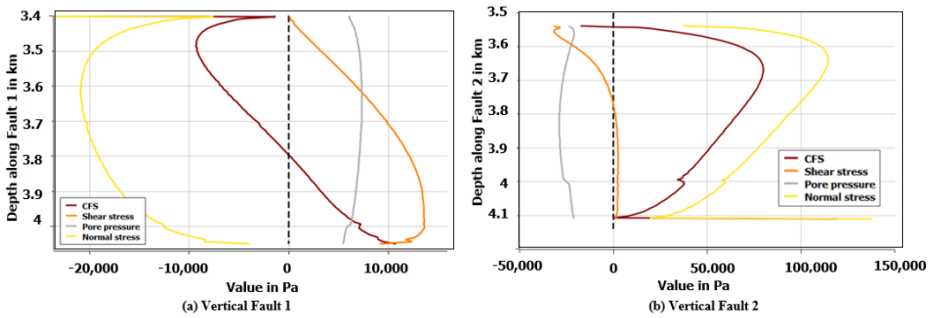

299

300 **Figure 5.** The variation of CFS, shear stress, normal stress, and pore pressure during HF along

301 the vertical faults: (a) Fault 1 and (b) Fault 2

302 4.2 Distance to HF operations

303 We consider that the location of Fault 2 is fixed and that of Fault 1 is variable and that the
304 distance between the last fluid mass source and Fault 1 is "d". If Fault 1 is less than 1.01 km away
305 from the HF operations, the fault will be affected by pore pressure diffusion caused by the
306 hydraulic fracturing operations. This leads to more destabilization of its shallower section.
307 However, if Fault 1 is more than 1.01 km away from the operations, the effect of the operations
308 will diminish. Four values for the distance between Fault 1 and the operations are adopted: $d = 0, 0.51, 1.01$ and 1.51 km. When the distance is 0 km, the fault intersects with the last hydraulic
310 fracturing mass source (**Fig. 7a**).

311 During the 4 stages, as Fault 1 becomes closer to the hydraulic fracturing operations, the
312 diffusion of pore pressure is facilitated (**Fig. 7**) and its CFS values become positive pointing to a
313 destabilized response (**Fig. 6a**) due to the combined effect of pore pressure and stresses.
314 Furthermore, as this distance decreases, the normal compressive stresses at the deeper part of the
315 fault decreases leading to its destabilizing, leaving a smaller part of the shallow section stable.
316 This explains positive CFS values of Fault 1 presented in **Fig. 6a**. When the fault intersects with
317 the hydraulic fracturing zone, Fault 1 is completely destabilized as it is entirely under very low
318 normal compressive stresses and relatively high pore pressure. On the contrary, if Fault 1 is
319 1.51 km away, most of Fault 1 is under compression and is stabilized while smaller part of its
320 deeper section is destabilized due to a lower compressive normal stress. To observe a response
321 that shows a stabilized upper part and destabilized lower part, which agrees with the seismic
322 observations, the distance between Fault 1 and the operations should be around 1.01 km. As for
323 Fault 2, the variation of CFS is barely affected by altering the distance of Fault 1 to the operations.
324 (**Fig. 6a**).

325 Having said that, when Fault 1 is 1.01 km away from the operations, its shallower sections
326 are under compression and show a stabilizing behavior (i.e., negative CFS) that agrees with the
327 lack of seismic events from observational data, and the deeper sections of Fault 1 are under lower
328 normal compressive stresses and show a destabilizing behavior (i.e., positive CFS), which
329 correlates with the observed seismic events. Otherwise, the response will not correlate with the
330 observed seismic events as Fault 1 will either be almost completely stabilized (at a distance
331 greater than 1.51 km) or destabilized (when the fault intersects with the HF operations).
332 Therefore, the position of the faults with respect to the location of the hydraulic fracturing

operations play an important role in the mechanisms affecting the fault response leading to induced earthquakes and in their spatiotemporal distribution.

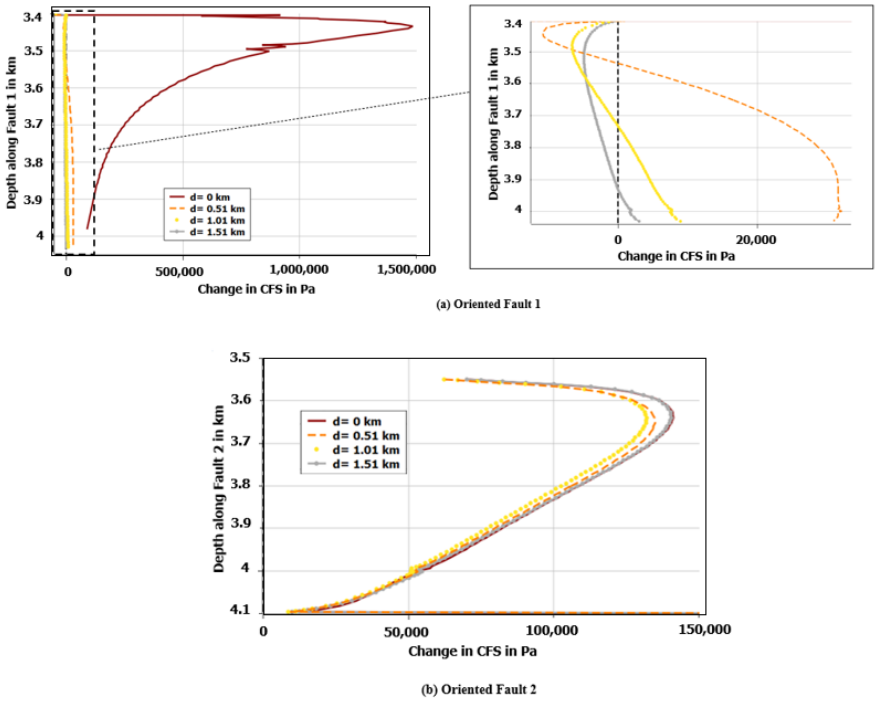

Figure 6. The variation of CFS during HF at different distances between Fault 1 and the hydraulic fractures along the oriented faults: (a) Fault 1 and (b) Fault 2

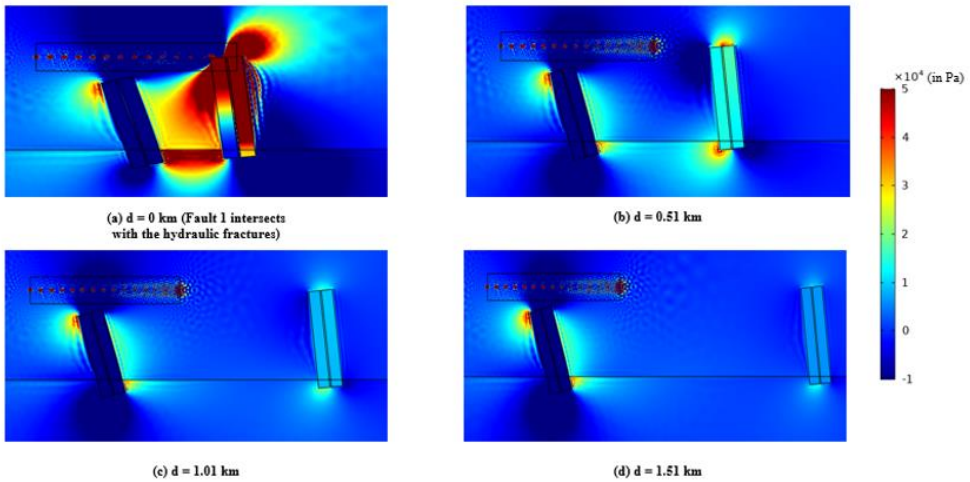

Figure 7. Coloured map showing the pore pressure diffusion at the end of HF at different distances (a) d= 0 km, (b) d= 0.51 km, (c) d= 1.01 km, and (d) d= 1.51 km

4.3 The width of the hydraulically fractured (HF) zone

To accurately simulate the effect of hydraulic fracturing operations, a zone is created around the hydraulic fractures (mass sources) which has a higher permeability and porosity than Duvernay shale. According to SM Energy company (2015), existing fractures can propagate up to 90 m because of the fluid injected at high pressures into the formation. The aim of this section is to evaluate the effect of the width of the HF zone on the variation of CFS along the critically stressed faults. We consider 3 scenarios: ignoring the permeability increase in the HF (**Fig. 8a**), the HF zone, with higher permeability than the host rock, does not intersect with Fault 2 (**Fig. 8b**), and the HF intersects with Fault 2 (**Fig. 8c**). The distance between Fault 1 and the operations is considered to be 1.01 km.

Fig. 9a shows the variations of CFS along Fault 2 for the 3 scenarios on the third day of HF. The highest CFS values are attained when the HF zone intersects with the damage zone of Fault 2. Since the HF zone and damage zone of Fault 2 have relatively high permeabilities (10^{-16} and 10^{-14}m^2, respectively), the propagation of the pore pressure is higher in comparison

to when no intersection exists (**Fig. 9b**). Consequently, the existence of a low permeability shale region between the hydraulically fractured zone and Fault 2 (**Fig. 8a and 7b**) acts as a barrier and delays the pore pressure diffusion along the fault. The slow perturbation leads to a decrease in the CFS values for cases (a) and (b) (**Fig. 9a**) especially that, during HF, the main mechanism affecting the fault response of Fault 2 is the pore pressure diffusion. The presence of HF zone does not affect the CFS values of Fault 1 since Fault 1 is not destabilized during HF by a direct increase in pore pressure.

It is important to note that it is highly unlikely that there was an intersection between Fault 2 and HF zone in the real case of Duvernay formation in Alberta. According to **Fig. 1**, the seismicity along Fault 2 during HF started in the deeper regions. If there was an intersection between Fault 2 and the HF zone, we expect to have seismicity start in the shallow sections.

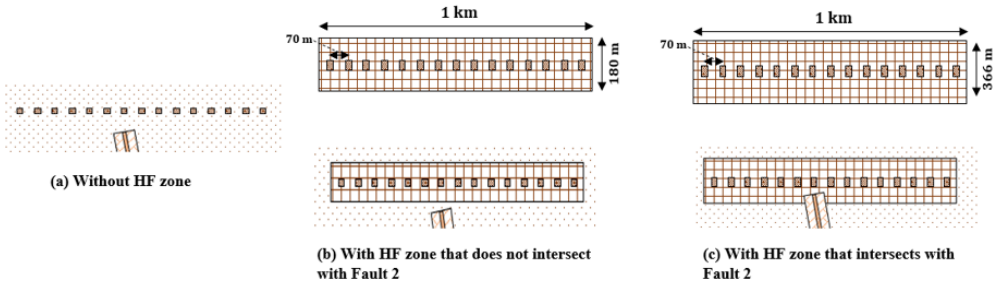

Figure 8. A close map showing the area around the hydraulic fractures and the shallow part of Fault 2 (a) without HF zone, (b) with HF zone that does not intersect with Fault 2 and (c) with HF zone that intersects with Fault 2

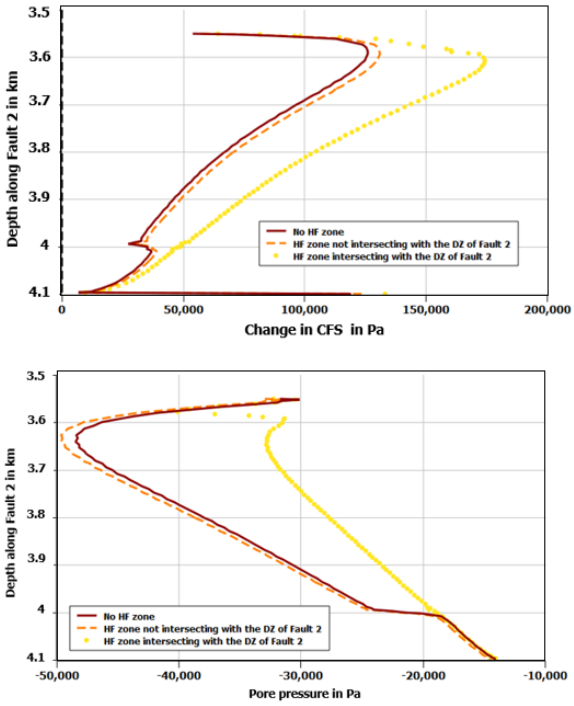

Figure 9. The variation of (a) CFS and (b) pore pressure on the third day of HF operations under different conditions: absence of HF zone (dark red), presence of HF zone that does not intersect with the damage zone (DZ) of Fault 2 (orange), and presence of HF zone that intersects with the DZ of Fault 2 (yellow)

4.4 Effect of fault architecture (width of the damage zone of Fault 1)

Depending on the location of the fluid perturbation with respect to the fault, the damage zones can play a significant role in the stabilization story. For the near fault, the damage zone plays the role of a hydraulic conduit to drive the increase in pore pressure to deeper regions of the fault. However, the width of the damage zone of the distant fault (Fault 1) might lead to decreasing the pore pressure along the fault by preventing pressure buildup and stress concentration. Therefore, four scenarios are considered where the width of the damage zone of Fault 1 (w_DZ) is varied between $0, 90, 150$ and 190 m. According to **Fig. 10a**, the deeper Fault 1 is more stable

when the damage zone is wider. **Fig. 10b** shows that the deeper section of Fault 1 is destabilized due to high shear stress relative to the shallower section of the fault. However, as the width of the damage zone increases, the pore pressure and shear stress decrease and the deeper section of the fault becomes more stabilized. The pore pressure in Fault 1 (**Fig. 10c**) is increased by the poroelastic effect and increase in the overall stresses with an indirect hydraulic connection. The more the pore fluids are trapped, the higher the pore pressure. A wider damage zone will allow a lateral diffusion resulting in the relaxation and the decrease of the pore fluid pressure around the fault. Therefore, the width of Fault 1 damage zone is expected to range between 100 and 160 m to yield a stress perturbation that is compatible with a response that correlates to the observed seismic events (stabilization during S1, S2 and S3 and destabilization of the shallow section during HF).

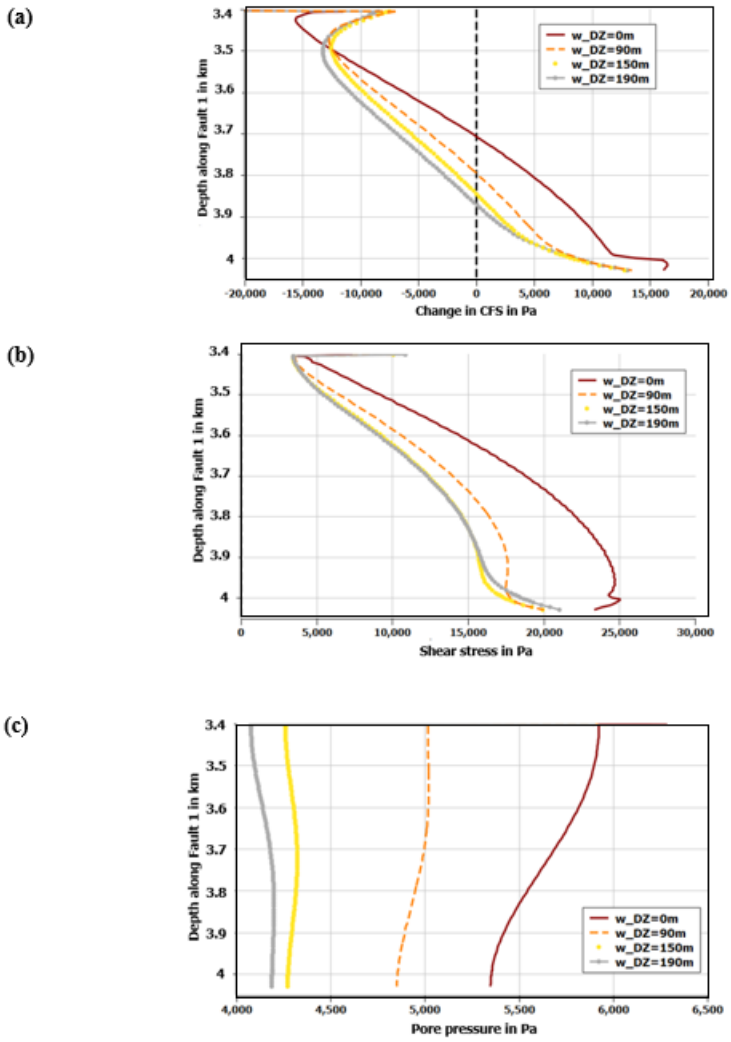

Figure 10. The variation of (a) CFS, (b) shear stress and (c) pore pressure during HF under different width of the damage zone (w_DZ) for Fault 1

4.5 Comparison to Fayetteville formation

A set of geological factors could have triggered the observed seismic events in the Duvernay formation, namely the proximity to the HF operations, the fault architecture and orientation, and the injection volumes and stages. In Fayetteville formation in north-central Arkansas, U.S., no seismic events have been reported during or after the hydraulic fracturing operations. Fayetteville formation is a Mississippian black clay shale along with interbedded fine-

grained limestones (McFarland, 2004). It contains around 41.6 Tcf of petroleum reserves (Arthur and Coughlin, 2008) and its age is almost equivalent to the Barnet Shale in Texas (Shelby, 2008). To compare, the total volume of fluid injected in the Fayetteville formation was around 400 $m^3/cluster$ while it was around $2{,}000\ m^3/cluster$ in the Duvernay formation. This plays a significant role in the rate and intensity of the increase in pore pressure and the stress perturbation and, therefore, the variation of CFS along the existing faults. In addition to that, the difference between the two case studies highlights the importance of the location of the existing faults relative to the hydraulic fractures. In the Fayetteville formation, two wells are operated next to a fault: one that is far (around 5 km away) and barely affects the stability of the fault and another close well whose total injected volume is very small in comparison to the Duvernay formation. Even if the hydraulic fracturing operations were close to the existing faults, the injection schedule (duration, rate, and volume of injection) plays a vital role in avoiding induced seismicity. According to Alghannam and Juanes (2020), the probability of the occurrence of seismic events increases in a shorter injection duration and a fixed injected volume as the case in the Duvernay formation.

5 Conclusions

The rate of injection and the volume of injected fluid play a major role in induced seismicity (Alghannam & Juanes, 2020). However, for a specific injection strategy, the hydrogeological factors that have a direct effect on the pore pressure and stress perturbation along the faults are the fault orientation, distance to the operations, the width of HF zone, and the fault's architecture. These factors made the geological setting critical for induced seismicity in the Duvernay formation in Alberta. Our results show that the mechanism affecting a distant fault response, during HF, is the shear stress rather than pore pressure diffusion while both factors play a significant role in destabilizing a close Fault. When pore pressure is not the main destabilizing

mechanism, the distance between the fault and the HF operations decides what part of the fault will be under a lower compressive stress and sometimes under extension, which affects its stability. Furthermore, the effect of the width of HF zone is insignificant unless it hydraulically intersects with the damage zone of a nearby fault; in that case, the pore pressure diffusion will be accelerated, and the fault will be destabilization will start in the shallower section. Finally, in a distant fault i.e., where indirect fluid perturbation is happening, the width of the damage zone plays an important role in stabilizing the fault by avoiding the pressure build up and entrapment and allowing the fluid to diffuse laterally, which leads to the decrease in shear stress and pore pressure perturbations. However, for a near fault, where direct fluid communication occurs, the damage zone plays the role of a conduit to diffuse pore pressure faster into the deeper regions of the fault.

Acknowledgments, Samples, and Data

The authors would like to thank Pr. James R. Rice, Dr. Tajuldeen Iwalewa, and Dr. Zhuo Yang from Harvard University for the fruitful discussions during the course of this research. This work is funded by the University Research Board at the American University of Beirut (*Award # 103780; Project # 24698).*

Data Availability Statement

The data related to this work can be accessed through the following link: https://dataverse.harvard.edu/dataset.xhtml?persistentId=doi:10.7910/DVN/2SVLHS

References

Alghannam, M. and Juanes, R. (2020), Understanding rate effects in injection-induced earthquakes. *Nature Communications*, 11(1), 1–6. doi: 10.1038/s41467-020-16860-y.

Arthur, D. J. and Coughlin, B. J. (2008), Hydraulic Fracturing Considerations for Natural Gas Wells of the Fayetteville Shale. 1–19. Available at: internal-pdf://arthur_fayetteville-0032732421/Arthur_Fayetteville.pdf.

Atkinson, G. M. et al. (2016), Hydraulic fracturing and seismicity in the western Canada sedimentary basin. *Seismological Research Letters*, 87(3), 631–647. doi: 10.1785/0220150263.

Bao, X. and Eaton, D. W. (2016), Fault activation by hydraulic fracturing in western Canada. *Science*, 354(6318), 1406–1409. doi: 10.1126/science.aag2583.

Benson, P. M. et al. (2020), Laboratory simulations of fluid-induced seismicity, hydraulic fracture, and fluid flow. *Geomechanics for Energy and the Environment*, 24, 100169. doi: 10.1016/j.gete.2019.100169.

Biot, M. A. (1941), General theory of three-dimensional consolidation. *Journal of Applied Physics*, 12(2), 155–164. doi: 10.1063/1.1712886.

Bommer, J.J. et al. (2006), Control of hazard due to seismicity induced by a hot fractured rock geothermal project. *Engineering Geology*. 83, 287–306. https://doi.org/10.1016/j.enggeo.2005.11.002

Brudzinski, M. R. and Kozłowska, M. (2019), Seismicity induced by hydraulic fracturing and wastewater disposal in the Appalachian Basin. USA: a review. *Acta Geophysica*, 67(1), 351–364. doi: 10.1007/s11600-019-00249-7.

Chang, K. W. and Segall, P. (2016), Injection-induced seismicity on basement faults including poroelastic stressing. *Journal of Geophysical Research: Solid Earth*, 121(4), 2708–2726. doi: 10.1002/2015JB012561.

Davies, R. et al. (2013), Induced seismicity and hydraulic fracturing for the recovery of hydrocarbons. *Marine and Petroleum Geology*, 45, 171–185. doi: 10.1016/j.marpetgeo.2013.03.016.

Davis, C. and Fisk, J. M. (2017), Mitigating Risks From Fracking-Related Earthquakes: Assessing State Regulatory Decisions. *Society and Natural Resources*, 30(8), 1009–1025. doi: 10.1080/08941920.2016.1273415.

Deng, F., Dixon, T. H. and Xie, S. (2020), Surface Deformation and Induced Seismicity Due to Fluid Injection and Oil and Gas Extraction in Western Texas. *Journal of Geophysical Research: Solid Earth*, 125(5), 1–22. doi: 10.1029/2019JB018962.

Deng, K., Liu, Y. and Harrington, R. M. (2016), Poroelastic stress triggering of the December 2013 Crooked Lake, Alberta, induced seismicity sequence. *Geophysical Research Letters*, 43(16), 8482–8491. doi: 10.1002/2016GL070421.

Ellsworth, W. L. (2013). 'Injection-Induced Earthquakes', 341(July), pp. 1–8.

Fan, Z., Eichhubl, P. and Gale, J. F. W. (2016), Geomechanical analysis of fluid injection and seismic fault slip for the Mw4.8 Timpson, Texas, earthquake sequence. *Journal of Geophysical Research: Solid Earth*, (April 2008), 3782–3803. doi: 10.1002/2015JB012608.Received.

Fan, Z., Eichhubl, P. and Newell, P. (2019), Basement Fault Reactivation by Fluid Injection Into

490 Sedimentary Reservoirs: Poroelastic Effects. *Journal of Geophysical Research: Solid Earth*,
491 124(7), 7354–7369. doi: 10.1029/2018JB017062.

492 Frohlich, C. (2012), Two-year survey comparing earthquake activity and injection-well locations
493 in the Barnett Shale, Texas. *Proceedings of the National Academy of Sciences of the United*
494 *States of America*, 109(35), 13934–13938. doi: 10.1073/pnas.1207728109.

495 Galloway, E. et al. (2018), Faults and associated karst collapse suggest conduits for fluid flow
496 that influence hydraulic fracturinginduced seismicity. *Proceedings of the National Academy of*
497 *Sciences of the United States of America*, 115(43), E10003–E10012. doi:
498 10.1073/pnas.1807549115.

499 Gudmundsson, A. (2004), Effects of Young's modulus on fault displacement. *Comptes Rendus -*
500 *Geoscience*, 336(1), 85–92. doi: 10.1016/j.crte.2003.09.018.

501 Healy, J. H. et al. (1968), The Denver Earthquakes. Disposal of waste fluids by injection into a
502 deep well has riggered earthquakes near Denver, Colorado. *Science*, 1301–1310.

503 Holland, A. A. (2013), Earthquakes triggered by hydraulic fracturing in south-central Oklahoma,
504 *Bulletin of the Seismological Society of America*, 103(3), 1784–1792. doi: 10.1785/0120120109.

505 Kleiner, S. and Aniekwe, O. (2019), The Duvernay Shale completion journey. *Society of*
506 *Petroleum Engineers - SPE Kuwait Oil and Gas Show and Conference 2019, KOGS 2019*, 1–7.
507 doi: 10.2118/198070-ms.

508 McFarland, J. D. (2004), Stratigraphic Summary of Arkansas. *Arkansas Geological Survey*
509 *Information Circular*, 44. Available at: http://www.geology.ar.gov/info_circulars/ic36.htm.

McGarr, A. (2014), Maximum magnitude earthquakes induced by fluid injection. *AGU: Journal of Geophysical Research, Solid Earth*, 119, 3678–3699. doi: 10.1002/2013JB010597.

McClure, M.W. et al. (2014), Correlations between formation properties and induced seismicity during high pressure injection into granitic rock, *Engineering Geology*. 175, 74–80. https://doi.org/10.1016/j.enggeo.2014.03.015

Mendecki, M.J. et al. (2020), Mining-triggered seismicity governed by a fold hinge zone: The Upper Silesian Coal Basin, Poland, *Engineering Geology.* 274. https://doi.org/10.1016/j.enggeo.2020.105728

Peduzzi, P. and Harding, R. (2013), Gas fracking: can we safely squeeze the rocks?. *Environmental Development*, 6(November), 86–99. doi: 10.1016/j.envdev.2012.12.001.

Preston, A., Garner, G. and Beavis, K. (2016), Duvernay Reserves and Resources Report. (December).

Rashedi, H. and Mahani, A. (2016), Data Analysis of Induced Seismicity in Western Canada. 2, 26–28.

Rice, J. R. and Cleary, M. P. (1976), Some basic stress diffusion solutions for fluid-saturated elastic porous media with compressible constituents. *Reviews of Geophysics*, 14(2), 227–241. doi: 10.1029/RG014i002p00227.

Rodríguez-pradilla, G. (2018), Reservoir Characterization of a Duvernay-Fox Creek Shale Reservoir using Seismic, Microseismic, and Well Log Data. *CSEG Recorder*, (June), 30–34.

Schultz, R. et al. (2015), Hydraulic Fracturing and the Crooked Lake Sequences: Insights

Gleaned From Regional Seismic Networks. *Geophysical Research Letters*, 261–308. doi: 10.1007/978-3-319-21314-9_8.

Schultz, R. *et al.* (2017), A seismological overview of the induced earthquakes in the Duvernay play near Fox Creek, Alberta. *Journal of Geophysical Research: Solid Earth*, 122(1), 492–505. doi: 10.1002/2016JB013570.

Schultz, R., Stern, V. and Gu, Y. J. (2014), An investigation of seismicity clustered near the Cordel Field, west central Alberta, and its relation to a nearby disposal well. *Journal of Geophysical Research: Solid Earth*, 119(4), 3410–3423. doi: 10.1002/2013JB010836.

Segall, P. and Lu, S. (2015), Injection-induced seismicity: Poroelastic and earthquake nucleation effects. *Journal of Geophysical Research: Solid Earth*, 120(7), 5082–5103. doi: 10.1002/2015JB012060.

Shelby, P. (2008), The Fayetteville Shale Play of North-Central Arkansas – A Project Update. Available at: http://www.geology.ar.gov/info_circulars/ic36.htm.

Stober, I. and Bucher, K. (2014), Hydraulic conductivity of fractured upper crust: insights from hydraulic tests in boreholes and ? Fluid-rock interaction in crystalline basement rocks, 2019–2021. doi: https://doi.orh.10.1111/gfl.12104.

Suckale, J. (2009), Induced Seismicity in Hydrocarbon Fields. *Advances in Geophysics*, 51(C), 55–106. doi: 10.1016/S0065-2687(09)05107-3.

Van Eijs et al. (2006), Correlation between hydrocarbon reservoir properties and induced seismicity in the Netherlands. *Engineering Geology*, 84, 99–111.

https://doi.org/10.1016/j.enggeo.2006.01.002

van Thienen-Visser, K. et al. (2018), Categorizing seismic risk for the onshore gas fields in the Netherlands. *Engineering Geology*, 237, 198–207. https://doi.org/10.1016/j.enggeo.2018.02.004

Villa, V. and Singh, R. P. (2020), Hydraulic fracturing operation for oil and gas production and associated earthquake activities across the USA. *Environmental Earth Sciences*, 79(11), 1–11. doi: 10.1007/s12665-020-09008-0.

Walsh, F. R. and Zoback, M. D. (2015), Oklahoma's recent earthquakes and saltwater disposal. *Science Advances*, 1(5). doi: 10.1126/sciadv.1500195.

Wang, H. F. (2000), Theory of linear poroelasticity with applications to geomechanics and hydrogeology. *Princeton University Press*.

Witherspoon, P.A. and Gale, J.E. (1977), Mechanical and hydraulic properties of rocks related to induced seismicity. *Engineering Geology*. 11, 23–55. https://doi.org/10.1016/0013-7952(77)90018-7

Wu, J.H. et al. (2017), An experimental study to characterize the initiation of the seismic-induced Tsaoling rock avalanche. *Engineering Geology*. 217, 110–121. https://doi.org/10.1016/j.enggeo.2016.12.015

Yehya, A., Yang, Z. and Rice, J. R. (2018), Effect of Fault Architecture and Permeability Evolution on Response to Fluid Injection. *Journal of Geophysical Research: Solid Earth*, 123(11), 9982–9997. doi: 10.1029/2018JB016550.

Zbinden, D. et al. (2017), On the physics-based processes behind production-induced seismicity

in natural gas fields. *Journal of Geophysical Research: Solid Earth*, 122(5), 3792–3812. doi: 10.1002/2017JB014003.

Zhao, B. (2018), Geomechanical Modelling of Induced Seismicity. *Thesis*, (August).

Captions

Figure 1. Cross section of a cluster showing the two strands of the fault system in the Duvernay formation (reproduced from Bao and Eaton (2016))

Figure 2. Model geometry with emphasis on (a) the hydraulic fracturing zone, and the geometry of (b) Fault 1 and (c) Fault 2

Figure 3. The variation of the CFS during the 4 stages (HF, S1, S2, S3) along the oriented faults: (a) Fault 1 and (b) Fault 2

Figure 4. The variation of CFS, shear stress, normal stress, and pore pressure along (a) oriented Fault 1 during HF and (b) oriented Fault 2 during S1

Figure 5. The variation of CFS, shear stress, normal stress, and pore pressure during HF along the vertical faults: (a) Fault 1 and (b) Fault 2

Figure 6. The variation of CFS during HF at different distances between Fault 1 and the hydraulic fractures along the oriented faults: (a) Fault 1 and (b) Fault 2

Figure 7. Coloured map showing the pore pressure diffusion at the end of HF at different distances (a) d= 0 km, (b) d= 0.51 km, (c) d= 1.01 km, and (d) d= 1.51 km

Figure 8. A close map showing the area around the hydraulic fractures and the shallow part of Fault 2 (a) without HF zone, (b) with HF zone that does not intersect with Fault 2 and (c) with HF zone that intersects with Fault 2

Figure 9. The variation of (a) CFS and (b) pore pressure on the third day of HF operations under different conditions: absence of HF zone (dark red), presence of HF zone that does not intersect with the damage zone (DZ) of Fault 2 (orange), and presence of HF zone that intersects with the DZ of Fault 2 (yellow)

Figure 10. The variation of (a) CFS, (b) shear stress and (c) pore pressure during HF under different width of the damage zone (w_DZ) for Fault 1

Table 1. Hydraulic properties of the geological components used in the numerical models

Table 2. Linear elastic properties of the geological components used in the numerical models

Table 3. Poroelastic property of the geological components used in the numerical models

Table 4. Fluid properties used in the numerical models